SPACE OBJECT ATTITUDE ESTIMATION USING SATELLITE LASER RANGING SIMULATIONS

S. Schneider(1), M. Steindorfer(1), P. Wang(1), F. Koidl(1), N. M. Trummer(1), and D. Fauland(1)

(1)Space Research Institute, Austrian Academy of Sciences, Lustbühelstraße 46, 8042, Graz, Austria, Email: sebastian.schneider@oeaw.ac.at

ABSTRACT

This work discusses a method to estimate a spacecraft's rotation axis and period from ground, supporting in-orbit-servicing or active space debris removal. It requires simultaneous observations from two Satellite Laser Ranging (SLR) stations of a target equipped with multiple Corner Cube Reflectors (CCR). The method was developed and tested using a SLR residual simulation tool where various input parameters like CCR pattern or rotational behavior can be altered. A vector between a known CCR and a second, initially unknown one, is estimated and the behavior over time is analyzed. The estimation is done by using the residual distance between the CCRs and the two perspectives yielded by the bi-static data. However, ambiguities occur which can be solved by adding a third SLR station into the equation or compare multiple passes.

Keywords: SLR Simulation; Attitude Estimation; Space Debris; Bi-Static Observation.

1. INTRODUCTION

Space objects are the sum off all human made objects launched into space ranging from active or dysfunctional satellites to the smallest particles. Smaller space debris are the result of disintegration, erosion or collisions which also pose a risk to active missions due to their high velocity of about 7 km/s in low Earth orbit [1][2]. Especially collisions of larger objects like active or inactive satellites create a large number of space debris of smaller size which contribute to the Kessler Syndrome [3]. Not only is an active satellite damaged or destroyed but also the newly created space debris is hard to observe, due to its smaller size. To reduce the probability of such collisions, space debris are regularly observed using techniques like radar or Satellite Laser Ranging (SLR) [4]. In addition to the continuous observations it is desired to reduce the overall production of new space debris to an absolute minimum as stated in the Space Debris Mitigation Guidelines established by the Inter-Agency Space Debris Committee [5]. Furthermore, according to [6] the European Space Agency (ESA) "*aims to completely stop the generation of debris in valuable orbits by 2030*", which should be archived by active and passive removal techniques. While passive techniques rely on natural forces like Earth's magnetic field or atmospheric drag, active techniques require an artificial force applied on the object to alter its orbit. There are various different active removal techniques like laser ablation, tethers-based or capturing [7]. The concept of the capturing technique is to actively apprehend a dysfunctional spacecraft (S/C) or space debris with a chaser S/C and change its path either to reach the graveyard orbit or force the it to deorbit. Currently the ESA and a Swiss company are working on the ClearSpace-1 mission which purpose it is to actively capture and alter the orbit of the upper part of a payload adapter [8]. In order to make this mission feasible the orbit and the attitude of the object has to be determined beforehand. Thereby the attitude estimation from ground is more energy efficient. The chaser has more time to adjust its orbit and attitude and is able to use natural forced like Earth's magnetic field. It is imperative that the attitude is known in order to successfully synchronize the rotation of the target with the chaser. This is essential to avoid any potential damage and the creation of additional space debris while captioning the target [9].

This work analysis a method for estimating the attitude of a space object equipped with Corner Cube Reflectors (CCR) by observing it with standard SLR techniques from two different stations simultaneously. This allows to have two different observation vectors and thereby point of views, which solutions can be compared and merged. For this purpose, the study analyses how the relative distance between two specific CCRs on the surface of a space object changes over time along the observation direction when viewed from two different angles. In order to realize the method, it is important that the SLR stations are able to reach a certain resolution in their measurements to be able to distinguish single CCRs on the surface of the S/C. Due to the expenditure of having two stations observe a suitable target simultaneously, a Space Research Institute's tool for SLR residual simulation [10] is used to simulate a rotating target with any given number and pattern of CCRs mounted on the surfaces. The goal is to estimate the rotation axis and period to a certain accuracy for the purpose of active space debris removal.

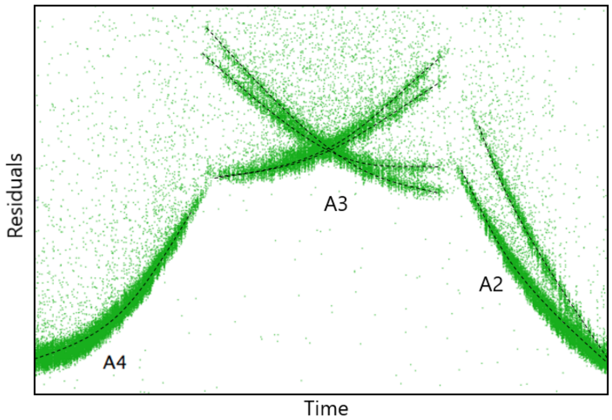

Figure 1. Measured TechnoSat pass residuals over time, as conducted by SLR station Graz [12]. The designations A4, A3 and A2 correspond to the individual surfaces on the S/C containing one, four and two CCR, respectively. The green dots represent valid returns and the dashed line highlight the mean residual of each CCR.

2. CORNER CUBE REFLECTORS SPATIAL CONFIGURATION

The number of CCRs and the arrangement in which they are mounted on the surfaces of an object is crucial for this method as it is important that every single CCR can be identified within the residuals. Therefore, the first step is to determine a suitable pattern which combines the uniqueness to be distinctive and the ability to be separable in the simulations and measurements.

2.1. Distinction of single Corner Cube Reflectors

Firstly, it is necessary to validate that distinctiveness can be achieved by standard SLR measurements. In Fig. 1 a Graz SLR station measurement of a TechnoSat pass is shown where post processing has already been done. The CCR pattern, the mounting distances and further information can be found in [12]. It can be seen that each CCR produced significant residual returns (green dots) which are marked with a black dashed line. Separation can be done for most parts of the pass if the pattern of the CCRs is considered. For example, the A3 surface: There are four CCRs arranged in a line, with two pairs positioned closer together. The distance between the pairs is 30 cm, and the distance between the outermost CCRs is 140 cm. TechnoSat is in a 600 km altitude orbit [11] which shows that CCR distinction is possible for S/C in low Earth orbit provided a certain mounting distance of the CCRs.

In order to estimate not only the attitude but also the current orientation it is important that the single CCRs can be differentiated and also be identified in the simulations and measurements. Therefore, a mainframe for the mounting pattern has to be established.

2.2. Corner Cube Reflector Placement Pattern

The primary goal is to establish a configuration in which each CCR is separable with absolute certainty. In theory any number of CCRs can be mounted as long as at least two CCRs can be identified, however, for practical reasons a configuration containing three CCRs was chosen.

The pattern was calculated using Eq. 1, which computes the maximum deviations in distances, d, between each CCR. This means that the distances should vary and be highly different to each other. This is done by maximizing the product of the differences between the distances from one CCR to each other. The advantage of calculating the product and not the sum is, that when two distances become too similar the difference becomes close to zero and the whole product becomes zero, which would not be a valid solution. The exponent, p, amplifies or dampens the influence of the pairwise differences. The higher the exponent gets, the larger and smaller differences contribute more and therefore get higher value. However, if it is too high, there is a risk that the entire product will become zero, because a factor smaller than 1 m can approach zero fairly quickly. Therefore, a compromise has to be found that gives value to the extremes but does not allow them to dominate. Furthermore, terms which would represent a distance variation to themselves are neglected and the positions of the CCRs (and their distances) have to be within the defined surface area. In this study, a rectangular surface was selected with the dimensions a and b being the constraints.

$$max \left(\prod_{i,j} (|d_i - d_j|)^p \right), \forall i \neq j, \forall d \mid d \leq \sqrt{a^2 + b^2} \tag{1}$$

The described problem in Eq. 1 was solved in Python with the solution, that all three CCRs are placed in a straight line. Two CCRs are located in opposite corners of the configuration, with one positioned at a distance of approximately one-fifth of the diagonal distance from a corner. The graphical illustration of the solution can be seen in Fig. 2, where the power, p, was chosen to be two. The characteristics of the surface rectangle does not have an influence on the diagonal, D, scaled solution. The resulting pattern allows the identification of each CCR in the residuals, except in the case where the surface is perpendicular to the observation vector. In this instance all CCR would have a similar distance to the observer. In all other circumstances, the red and green CCR are closer together than the blue one. Furthermore, the green CCR will always be positioned between the red and blue CCR. This behavior can be seen in an example simulation in Fig. 3. For all further examples this pattern will be used. Dependent on the SLR station's accuracy and measurement quality the minimum distance between two CCRs varies. However, as seen in Fig. 1, 30 cm is enough for Graz SLR station.

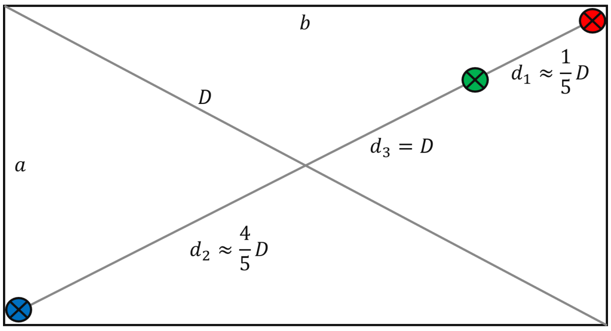

Figure 2. Calculated CCR pattern using Eq. 1 with power of 2 on a rectangular surface of a S/C. Blue, green and red circles with a cross are the CCRs. The labels a and b define the dimension of the rectangle and d_1, d_2 and d_3 are the distances between the CCRs which refer to the diagonal, D.

3. RESIDUAL SIMULATION TOOL

The Residual Simulation Tool (RST) calculates the observed-minus-calculated residuals to every single CCR based on a Two Line Element (TLE) orbit prediction. The necessary input file contains the information the simulation needs to compute a valid output, like the rotation parameters or the CCR position and orientation file path. In addition, a normal distributed noise, the CCR field of view (FOV) or a center of mass (CoM) offset can be chosen. More detailed information can be found in [10]. The RST was programmed in Python and is designed in a way that only the input file and the file which contains the CCR position and orientation has to be adapted before starting the simulation. In the input file the reference coordinate frame (RCF) can be chosen, which defines the frame for the rest of the simulation and the output. As the TLE files used are the one of actual satellite passes, the NORAD-ID as well as the start and end time of the pass have to be be added in order to automatically download the TLE file from SpaceTrack[1]. The basic structure of the RST is divided into eight sections:

- Definition of the input file (JSON format)
- Definition of pass time (elevation above 0°)
- Download TLE or use stored one
- Read station coordinates and velocity (Sinex files from CDDIS[2])
- Coordinate transformations
- Lagrange interpolation
- Read CCR position, normal vector and FOV
- Rotate CCR around fixed axis in the RCF

[1] www.space-track.org
[2] www.cddis.nasa.gov

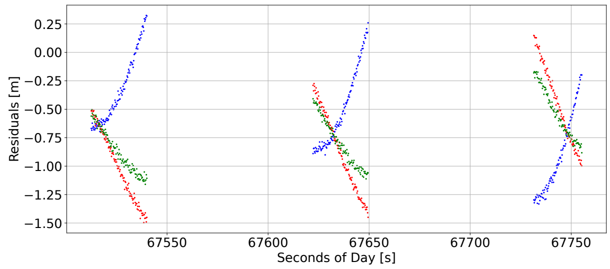

Figure 3. Example simulation of a TechnoSat pass with noise added. The Y-axis shows the observed-minus-calculated residuals which are the length deviations to the CoM in observation vector direction. The X-axis shows the seconds of day. The colored dots are the returns of the single CCRs. The CCR placement pattern is described in section 2.2 and the same color code is used.

The RST output comprises two main components: A graphical representation and data files that can be utilised for subsequent calculations. An example for the graphical representation can be seen in Fig. 3, where a TechnoSat pass with noise was simulated. The gaps in the residuals occur because CCRs where only placed on one face of the S/C. Therefore, whenever this face is not visible to the observer (observation vector it outside the FOV) no residuals where generated. Most of the residuals are negative because they represent the distance variation in observation vector direction relative to the CoM. The overwhelming time, the surface is orientated in the direction of the observer, which means that the surface is closer to the observer than the CoM, therefore generating negative residuals. The simulated output data includes the observation vector, residual and pass data, rotation information and normal vectors of the CCR at every time step.

4. ATTITUDE ESTIMATION

The attitude of a space object is defined by three components: Rotation axis, rotation period and orientation, defined in a reference frame. The requirements, assumptions and method will be discussed in this section to achieve the attitude estimation from ground using bi-static SLR residual simulation.

4.1. Requirements and Assumptions

There are some requirements and assumptions that have to be made in order to estimate the attitude. They are illustrated in Fig. 4, where a bi-static SLR measurement in sketched and explained.

- **Two identifiable CCRs**
  It is required to identify at least two CCR per surface in the simulated or measured residuals. One possibility how to achieve this is explained in section 2.2,

however any pattern with any number of CCRs is suitable provided two of them can be identified. If the orientation of the S/C is also of interest it is necessary to vary the pattern on each surface that allows face distinction.

- **Bi-static SLR observations**
  The space object has to be observed from at least two SLR stations simultaneously with an accuracy high enough to be able to calculate the residual differences between the singe CCRs. In real measurements campaigns however, measurements will hardly be measured at the exact same time due to clock errors or offsets. To counteract, the data points of each station will have to be interpolated, using e.g. a least squares adjustment. The establishment of three stations would be advantageous to eliminate ambiguities. However, the implementation of a campaign involving three stations is challenging due to weather-related limitations and measurement uncertainties.

- **Observation vector parallel to every point on the surface**
  It is assumed that the observation vector stays parallel, regardless of which part of the surface is observed. Therefore, the laser beam incident angle is equal regardless which CCR on the surface is currently under investigation. Due to the significant distance to the S/C, the minor angular deviations can be neglected.

- **Fixed rotation axis**
  For the estimation it is assumed that the rotation axis of the target is fixed with respect to the RCF and will not change over time. However, the axis can change due to free tumbling motion of objects. The method would perfectly allow to monitor those changes over time, which could be an option for the future experiments and simulation tests.

4.2. Simultaneous Observation

When talking about simultaneous observation it is important that both stations are far enough from each other to produce significant differences in the residuals. To demonstrate that a relatively small distance can result in measurable deviations, the same TechnoSat pass was simulated in Fig. 5, once from the perspective of the SLR station in Graz and once from the perspective of the SLR station in Wettzell. Afterwards the results where compared, showing differences up to 0.3 m. This value is significantly above the SLR measurement accuracy, which is for most SLR stations lower than 1 cm up to 5 cm [13]. These deviations are the result of the geographical distance of approximately 300 km between the two stations. The distance impacts directly the orientation of the observation vector, thus the incident angle.

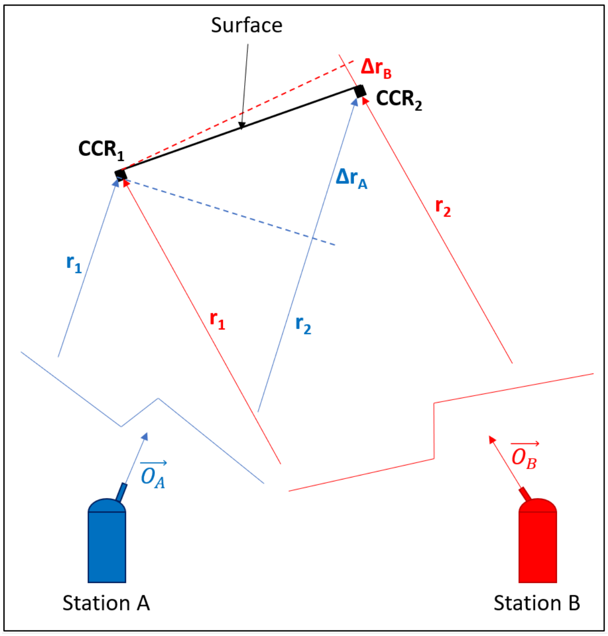

Figure 4. Schematic of bi-static observations which fulfill the requirements and assumptions. Two CCRs can be identified and their residual differences, $\Delta r = |r_1 - r_2|$, can be measured separately. The measurements take place simultaneously while the observation vector, $\vec{O}$, stays parallel for each station, A and B.

4.3. Calculation of a Surface-Vector

The objective is to estimate a vector pointing from one CCR to another. It is essential that these two reflectors can be identified within the measured or simulated residuals. As this vector is located on the surface of an object, it is referred to as a surface-vector. Based on the behavior over time, conclusions can be drawn about the attitude. The required data to perform the calculations are the residuals, CCR positioning on the surface, the observation vector and the epoch. The following list will describe the main steps which are necessary to calculate the surface-vector per time step.

- **Residual differences**
  Firstly, the residual differences between the two CCRs are calculated every time step and for both stations. The residual difference, Δr, is illustrated in Fig. 4 and can be calculated by subtracting the residuals of both CCRs. If the difference is very small, the surface is close to be perpendicular to the observation vector.

- **Centering one CCR**
  Secondly, the RCF's center of origin has to be shifted to the position of the designated first CCR. It is mandatory that the designated CCR is identical for both stations.

- **Radius of potential circular position**
  Thirdly, using geometric relations a circular area can

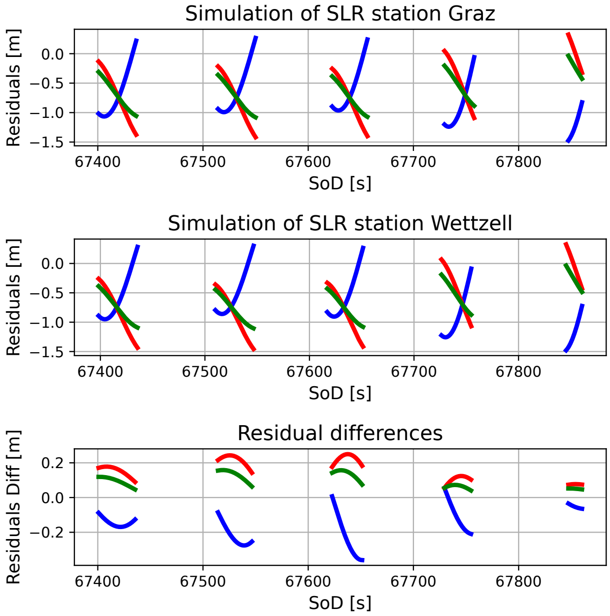

Figure 5. Top and mid: Simulated residuals from SLR station Graz and Wettzell, respectively, with X-axis being the Seconds of Day and the Y-axis the simulated-minus-calculated residuals; Bottom: Residual differences between both simulations where the Y-axis shows the residual differences; The orbit was calculated by using a TLE file from a TechnoSat pass. Graz and Wettzell are approximately 300 km apart which lead to residual differences up to 0.3 m.

be calculated on which the second CCR must lie, which is marked by the black circle where the CCR_3 lies on. This is illustrated on the left side of Fig. 6. Δr is the residual difference, d the surface distance between both CCRs, R the radius of the resulting circle and α the incident angle of the incoming laser beam. Δr is pointing in the observation vector direction and is perpendicular to the plane the circle is positioned on. Simple trigonometric relations can be applied to calculate Δr, thereby obtaining an approximate tilt of the surface. However, no orientation information is provided so far.

- **Intersection of circles**
  If the previous steps are done for both stations the resulting circles can be intersected. As a result, one or two intersection points are calculated, illustrated on the right side of Fig. 6, marked by the red crosses. $CCR_{3,1}$ and $CCR_{3,2}$ are the two potential positions of a second CCR and v_1 and v_2 the two potential surface-vectors.

- **Ambiguity of the surface-vector**
  This ambiguity can be resolved for example by adding the data of a third SLR station or analyzing a number of revolutions and passes. However, for the further purpose of this study this ambiguity is largely neglected to further investigate the rotation parameters.

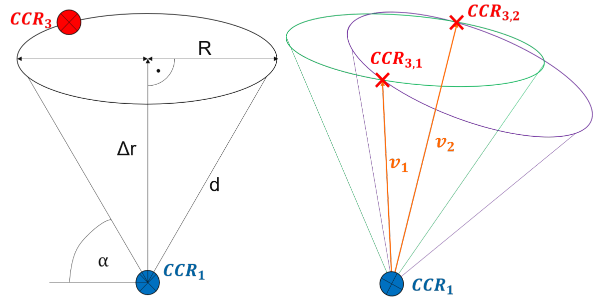

Figure 6. Left: A schematic representation of the potential circular relative position of a second CCR, example position marked red, seen from one station. R is the radius of the circle, Δr the residual difference, d the mounting distance and α the laser beam incident angle; Right: Both stations create a potential circular position which can be intersected to constrain the potential position to two points marked with a red cross. The connecting vectors are called surface-vectors and are represented by v_1 and v_2.

4.4. Surface-Vector-Propagation

When performing the steps described in section 4.3 for every time step, the surface-vector will propagate and rotate during the pass. For calculation and representation reasons the data is separated in single chunks. In this context, a chunk refers to a segment of a pass during which the surface remains continuously visible, occurring once per revolution. On the left side of Fig. 7 an example of a chunk is plotted containing both possible solutions, marked in the same color code to represent the impossibility of direct distinctness. To stay consistent the same CCR pattern and pass were used to generate the surface-vector as in the previous examples. However, the two different curves of the surface-vector can be clearly recognized visually. Yet, the two solutions are represented by a mixed data set and therefore must be separated first, to perform further analysis. By performing data editing like outlier removal, Euler step interpolation, cone filtering and proximity analysis the two curves can be separated. To apply these methods some default values, have to defined to begin the analysis. Data points will be removed if they have no neighbor in proximity less than 0.1 m (outlier removal). The subsequent initial point for finding the next data point is 0.01 m in the trending direction (Euler step). The permitted area in which the following point may be located is defined by a cone centered around the Euler step vector, with an opening defined by the ratio of the cone's height to the radius of the corresponding circular base. The default value is 25 (cone filtering). If no new data point can be found within proximity of less than 0.1 m the curve calculated so far is saved as a section (proximity). These methods can lead to a number of sections within the respective solution. Therefore, a spline of the order 1, 3 or 5 is fitted through the data points of one section and is extrapolated. The mean normal distance between the generated spline and the other sections is compared and, if the value is low enough, merged with

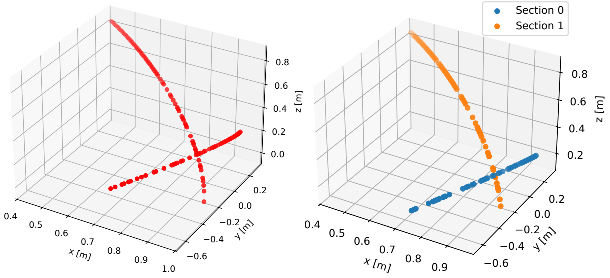

Figure 7. Left: Single Chunk where outliers are already removed. Solutions are not separated due to the mixed data sets; Right: Separated Chunk after performing Euler step interpolation, cone filtering and proximity analysis; The data shows the possible positions of the second CCR while the first is located at the center of origin.

the initial section. This step is iterated over all sections until one or two solutions remain. The result can be seen in Fig. 7 on the right side: The solution and ambiguity are separated from each other.

4.5. From Surface-Vector to Attitude

In this section the focus lies on the solution and not its ambiguity. Firstly, a least squares adjustment [14] of the second CCR's positions has to be performed to get a smooth movement during the pass. The CCR will move along a spiral: Circular due to the rotation and forward due to the orbit propagation. The rotation axis is in the center of the spiral and can be estimated by calculating a mean vector which is perpendicular to the vectors which connect the positions of the second CCR in each time step. The estimation of the mean rotation axis, $\overline{r_a}$, is given in Eq. 2, where N is the total number of connection vectors, which are labeled $\vec{d_i}$.

$$\overline{r_a} = \frac{\sum_{i=0}^{N-1} \vec{d_i} \times \overrightarrow{d_{i+1}}}{N-1} \tag{2}$$

The connection vectors can be calculated by subtracting the subsequent from the initial surface-vector. The calculation is shown Eq. 3 and must be applied for each time step the surface is visible.

$$\vec{d_i} = \vec{s_i} - \overrightarrow{s_{i+1}} \tag{3}$$

In Fig. 8, a schematic illustrates the initial situation this calculation is based on. The surface-vectors, $\vec{s_i}$, point to the position of the second CCR_2 every time step, i. Note that this is a projected illustration, a vector perpendicular to the surface-vectors might not point towards the observer direction, thus does not represent the rotation vector. This method is working to a good extent if the data points are well distributed on the spiral. However, if

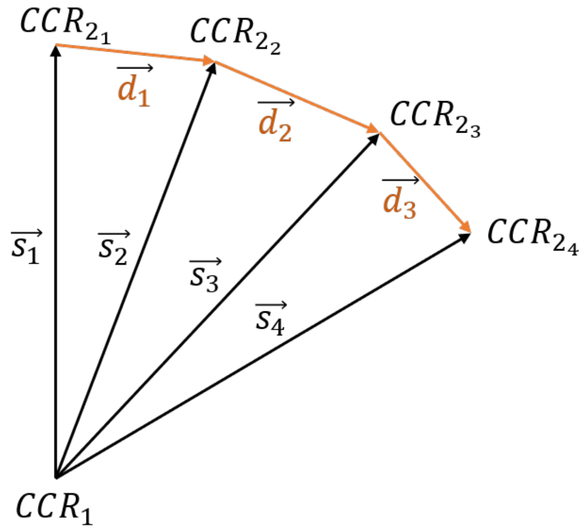

Figure 8. Schematic of surface-vectors, $\vec{s_i}$, pointing from the initial CCR, CCR_1, at each time step, i, to the second CCR, CCR_2. The position propagates circular and in orbit direction (along track) over time which results in a helix.

little data points are available and they are focused on a small portion of the spiral the RANSAC (Random Sample Consensus) method [15] to fit the spiral center axis is more suitable.

Now that the rotation axis is known the rotation period can be calculated. Due to the propagation on a spiral the surface-vectors are distorted and do not represent a perfect circular motion which would describe the rotation of the object. This effect can be seen in Fig. 9. To counteract this, a plane is created which is perpendicular to the estimated rotation axis. The surface-vector will now be projected on the newly established plane. While the not projected surface-vector point to the CCRs propagating on a spiral, the new projected surface-vectors, $\hat{s}[t]$, will point to the projected $CCR_2[t]$ positions, which propagate on a circle. The time passed between the two measurements is known and the angle between the two corresponding projected surface-vectors can be calculated. Thus, the time needed to fulfill a full revolution can be computed, which corresponds to the true rotation period. This is done for each time step and then the mean value is computed, which is given in Eq. 4, where t is the time between each step.

$$\tau = mean\left(\frac{2\pi * t}{cos^{-1}\left(\frac{\vec{\hat{s}_i} \cdot \overrightarrow{\hat{s}_{i+1}}}{|\vec{\hat{s}_i}| * |\overrightarrow{\hat{s}_{i+1}}|}\right)}\right) \tag{4}$$

In theory using this method the attitude of a space object can be measured. However due to lack of resources the preliminary results are limited to simulated data. The first part of the attitude is defined by the rotation axis, which can be estimated with the given method to an accuracy

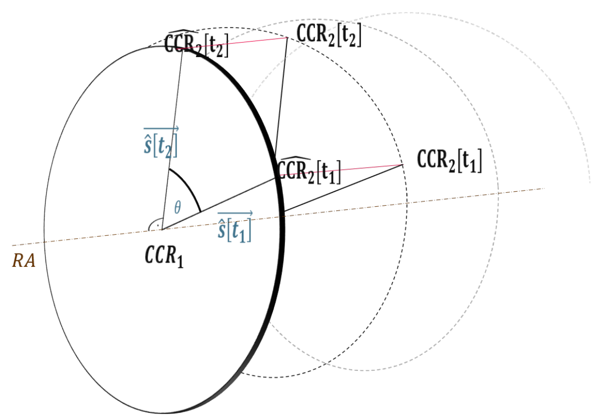

Figure 9. Schematic of the spiral propagation of the second CCR through space. Surface-vectors are projected, ŝ[t], on a plane perpendicular to the estimated rotation axis to exclude the objects forward movement. ŝ is now rotating in a circular path, so the rotation period can be computed.

of below 50 μrad for a single-step calculation and below 0.1 μrad for the mean value (actual estimated axis). The result of the angular deviation before applying the mean function (single-step) for a specific example can be seen in Fig. 10. The single-step rotation axis is $r_{\mathrm{i}} = \overrightarrow{d_{\mathrm{i}}} \times \overrightarrow{d_{\mathrm{i+1}}}$ at each time step separately. The deviations are normal distributed, which allows the conclusion that they are caused by normal distributed noise and round-off-errors of the simulation tool and the attitude calculation itself. However, in the shown example the defined rotation axis was [1, 1, 0], in the RCF, and the estimated mean rotation axis is $[0.\dot{9}, 1 + 2*10^{-7}, -1.6*10^{-6}]$. This corresponds to a relative deviation of less than 10^{-6} %. Should a pass be observed where more revolutions are visible, the ambiguity can be resolved, because the true solution of the rotation axis will always be similar, while the ambiguity will vary with each observation and revolution.
After estimating the rotation axis, the rotation period can be calculated using Eq. 4. In Fig. 11 the rotation period at each time step of an example is plotted, where simulated rotation period was set to be 120 s. In this estimation the mean rotation period is 119.999 s, which corresponds to a relative deviation of 0.001 %, after removing certain outliers. Especially in regions where the surface is close to be perpendicular to the observation vector the estimation can become unstable, because the residual differences get close to zero. Minor impacts of this effect can be seen around 67420 SoD and 67530 SoD.

In theory the method should be able to estimate the rotational behavior provided a suitable CCR pattern and SLR stations which high accuracy measurement capabilities. The influence of measurement uncertainties and clock errors as well of station distances will be subject of further studies.

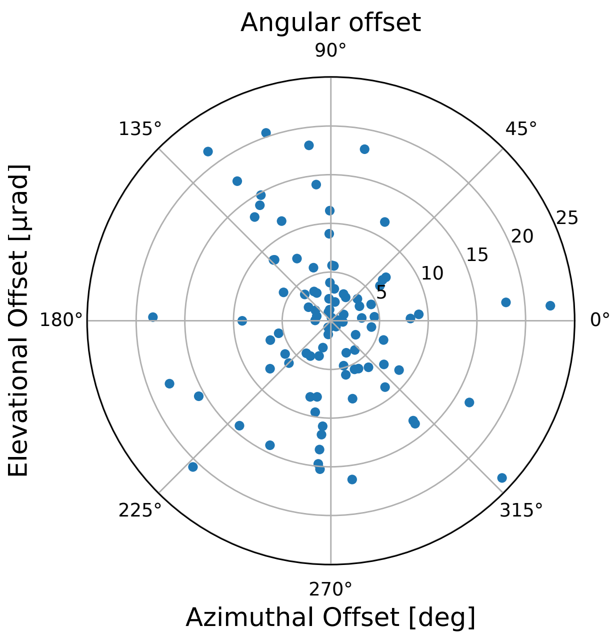

Figure 10. Angular deviation example of the rotation axis for a single-step calculation, result of Eq. 2 without computing the mean value. The example TechnoSat pass uses the explained CCR pattern. The deviations are normal distributed and below 25 μrad in this case, which can be related to noise and round-off errors. More revolutions can help to increase the accuracy of the results.

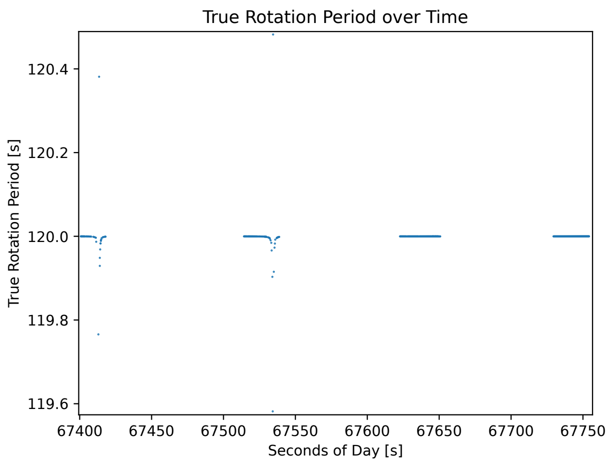

Figure 11. Example of a true rotation period estimation over time. At each time step the rotation period was calculated using Eq. 4 without the mean function. The gaps in the data are the sectors where the surface with CCRs mounted are not visible to the observer. Larger deviations occur in the areas where the surface is close to be perpendicular to the observation vector.

5. SUMMARY AND OUTLOOK

This study demonstrates the feasibility of using bi-static SLR to estimate the attitude of certain space objects where CCRs are mounted in a specific pattern. It is shown that one suitable pattern for making each CCR identifiable consists of three CCRs in a line, with two positioned closer together. Identification is only impossible when the surface is nearly perpendicular to the observer. Observing the objects from two different angles through bi-static measurements proves to be crucial for gaining additional information, as the two datasets can be compared. The variations in these datasets enable attitude calculation. However, due to the ambiguities inherent in this method, further assessment is required. When observing a single revolution, these ambiguities cannot be resolved using the standard method. It is necessary to analyze multiple revolutions and passes to identify the actual solution and eliminate ambiguities. Resolving these ambiguities within a single revolution would require a third SLR station. Observations involving three SLR stations could even enable real-time attitude estimation, which could be necessary or beneficial when a satellite is approaching space debris for removal.

In reality, the accuracy of the estimated attitude depends largely on the quality of the SLR station measurements. Additionally, the observing stations require good weather conditions, which often poses a challenge and may make bi-static observations difficult to plan. This challenge would be even greater when considering tri-static observations.

In the future, the methods developed in this study could be implemented in a variety of applications. The increasing amount of space debris is becoming a growing concern for both commercial and governmental space agencies. Therefore, technologies such as SLR based attitude determination will play a significant role in future debris removal missions. The ability to precisely predict the rotation and attitude of space debris from the ground will be crucial for planning removal missions and avoiding collisions. This, in turn, will allow operational satellites to remain in orbit with minimal need for repeated collision avoidance maneuvers. In this context, the thesis has demonstrated that SLR, particularly bi-static SLR, is a valuable and viable technique for attitude determination of defunct satellites and space debris. While much work remains to be done, this study provides a strong foundation for further research in this field and may, in the future, make a significant contribution to space debris mitigation.

Future steps and further research are needed to establish this method as a standard procedure. An important question is how close two observing stations can be while still producing meaningful attitude estimations. If it is possible to have two or even three SLR stations within a few kilometers of each other, a single institute could operate them, significantly simplifying observation campaigns. Furthermore, stations within the same weather region would have a much higher probability of successful attitude estimation. An essential next step is to conduct a test campaign to validate the feasibility of the method using real measurements. Potential targets include TechnoSat and the SNET satellites, as both have CCRs mounted on all surfaces, with one surface featuring the CCR pattern outlined in this study. Additionally, it is necessary to examine how timing correlation errors in bi-static measurements affect the accuracy of attitude estimation. Further research could also explore how bi-static SLR data might be applied to other fields of interest.

DISCLOSURE

The authors used DeepL Write (by DeepL GmbH) and ChatGPT (by OpenAI) to assist with language editing and to improve grammar, style, and clarity during the preparation of this manuscript. All AI-assisted suggestions were critically reviewed and revised by the authors, who take full responsibility for the content and accuracy of the final version.

REFERENCES

1. Rayal, F., Hartani, R., Mendes, A., Cables, A. (2020). *Defining the Synergies between LEO Satellite Constellations and Submarine Cables*. Xona Partners Report, 1(1), 1-20.
2. Sylvestre, H. & Parama, V.R. (2017). *Space Debris: Reasons, types, impacts and management*. IJRSP 46(1), 20-26.
3. Kessler, D. J. & Cour-Palais, B. G. (1978). *Collision frequency of artificial satellites: The creation of a debris belt*. Journal of Geophysical Research: Space Physics, 83, 2637–2646.
4. Mehrholz, D., Leushacke, L., Flury, W., Jehn, R., Klinkrad, H., and Landgraf, M. (2002). *Detecting, tracking and imaging space debris*. ESA Bulletin (0376-4265), 109, 128-134.
5. Yakovlev, M. (2005). *The "iadc space debris mitigation guidelines" and supporting documents*. 4th European Conference on Space Debris. ESA Publications Division, European Space Agency, Noordwijk, The Netherlands, 591-597.
6. Sorares, T., Serrano, S. M., Flohrer, T., Cattani, B. M., de Courson, S.-A, Suriani, L., Turner, C. (2023). *ESA's Zero Debris Approach: A Responsible Path to Mittigate Space Debris in Valuable Orbits*. LPI Contributions, 2852, 6059
7. Priyant, C. M., Kamath, S. (2019). *Review of Active Space Debris Removal Methods*. Space Policy, 47, 194-206.
8. Biesbroek, R., Aziz, S., Wolahan, A., Cipolla, S. F., Richard-Noca, M., Piguet, L. (2021). *The clearspace-1 mission: ESA and clearspace team up to remove debris*. In Proceeding 8th European Conference on Space Debris, pp1-3.

9. Liu, E., Yang, Y., and Yan, Y. (2020). *Spacecraft Attitude Tracking for space debris removal using adaptive fuzzy sliding mode control*. Aerospace Science and Technology, 107, 106310.

10. Schneider, S., Steindorfer, M., Koidl, F., Wang, P., Jonglez, C., Barschke, M., Sorares, T., Padilla, E. (2022). *Reflector-based Attitude Detection System - SLR Residual Simulation Tool*. In Proceeding Clean Space Industry Days, Noordwijk, The Netherlands.

11. Barschke, M., Werner, P., Gordon, K., Lehmann, M., Frese, W., Noack, D., Grunwaldt, L., Kirchner, G., Wang, P., Schlepp, B. (2018), *Initial Results from the TechnoSat in-Orbit Demonstration Mission*. 32nd Annual AIAA/USU Conference on Small Satellites, Logan, Utah, USA, 126-136.

12. Wang, P., Almer, H., Kirchner, G., Koidl, F., Steindorfer, M. (2018). *kHz SLR Application on the Attitude Analysis of TechnoSat*. In Proceeding 21st International Workshop on Laser Ranging, Canberra, Australia.

13. Selvan, K., Siemuri, A., Prol, F.S., Välisuo, P., Bhuiyan, M. Z. H., Kuusniemi, H. (2023). *Precise orbit determination of LEO satellites: a systematic review*. GPS Solutions, 27(4), 178.

14. Huaan, F. (1997). *Theory of errors and least squares adjustment*. Royal Institute of Technology, Sweden.

15. Derpanis, K. G. (2010). *Overview of the RANSAC Algorithm*. Image Rochester NY, 4(1), 2-3.